

● *Original Contribution*

## VIBRATION SONOELASTOGRAPHY AND THE DETECTABILITY OF LESIONS

KEVIN J. PARKER,\* DONGSHAN FU,\* SHERYL M. GRACESWKI,<sup>†</sup> FAI YEUNG,\* and  
STEPHEN F. LEVINSON\*<sup>‡</sup>

Departments of \*Electrical and Computer Engineering, <sup>†</sup>Mechanical Engineering, and <sup>‡</sup>Physical Medicine and Rehabilitation, University of Rochester, Rochester, NY 14627 USA

(Received 16 March 1998; in final form 16 July 1998)

**Abstract**—Vibration sonoelastography has been developed for the detection of hard lesions in relatively soft tissue. The basic concept is to propagate low-amplitude and low-frequency shear waves (with displacements below 0.1 mm and frequencies typically below 1000 Hz) through deep organs, and displaying the vibration response in real-time using advanced color Doppler imaging techniques. A hard inhomogeneity, such as a tumor, will produce a localized disturbance in the vibration pattern, forming the basis for detection even when the tumor is isoechoic on B-scan images. This paper focuses on the important quantitative issues concerning the detectability or inherent contrast of lesions. The specific factors of lesion size, relative stiffness and vibration frequency are studied using theoretical models, finite element methods and experimental measurements on tissue-mimicking materials. The results indicate that detectability increases with vibration (shear wave) frequency; however, loss mechanisms ultimately limit the penetration of higher vibration frequencies (in the kHz range). © 1998 World Federation for Ultrasound in Medicine & Biology.

**Key Words:** Sonoelasticity, Sonoelastography, Ultrasound, Doppler, Shear waves, Vibration, Tumor detection, Tissue viscoelastic properties.

### INTRODUCTION

Vibration sonoelasticity imaging has been proposed for detection of hard lesions (Lerner et al. 1988, 1990; Parker et al. 1990; Yamakoshi et al. 1990; Gao et al. 1995, 1997) and also for the study of tissue viscoelastic properties (Levinson et al. 1995). In these methods, the amplitude and/or phase of vibration of the tissue is estimated and displayed using ultrasound pulse echo techniques specially designed for the Doppler signal of vibrating targets (Huang et al. 1990, 1992; Yamakoshi et al. 1990).

Other independent work has centered on estimating tissue properties using incremental compression of tissues (Ophir et al. 1991; O'Donnell et al. 1994; Skovoroda et al. 1994). The literature in this field has been reviewed in recent articles (Gao et al. 1996; Ophir et al. 1997), and is rapidly growing. Extensions to other modalities and many anatomical structures, such as the eye, are described in one review (Gao et al. 1996).

A theoretical framework has been established for the detection of inhomogeneities in a vibrating medium (Gao et al. 1995, 1997) with application to the liver, the prostate and other organs. Here, this framework will be extended to include a detailed treatment of lesion detectability. This paper examines theoretical relationships, along with new finite element models and experiments using tissue-mimicking materials, to establish the fundamental concepts and quantitative results pertaining to the issue of detectability of a lesion in an otherwise homogeneous elastic tissue medium. Specifically, we examine the localized change in vibration that is produced in a tissue-mimicking material as a function of the relative lesion elasticity, the vibration frequency and the lesion size. This localized change in vibration is quantified and forms the basis for a discussion of detectability and lesion contrast. These results provide guidelines for, and establish a relationship between, increased vibration frequency and increased detectability. However, in practical systems, the losses associated with higher vibration frequencies (in the kHz range) will place a practical limit on the choice of vibration frequency and, hence, the detectability of a small elastic inhomogeneity.

Address correspondence to: Kevin J. Parker, Department of Electrical and Computer Engineering, University of Rochester, Rochester, NY 14627, USA. E-mail: parker@ece.rochester.edu

## THEORY

For a linear viscoelastic and isotropic 3-D structure, solutions for the wave motion cannot be obtained analytically, except for the simplest geometry and boundary conditions. These problems are often made tractable by incorporating some assumptions and simplifications. Gao et al. (1995) have formulated a mathematical model for vibration amplitude sonoelastography. A lesion is modeled as an elastic inhomogeneity inside a lossy homogeneous elastic medium. The homogeneous medium has constant stiffness  $E_0$ , and the small inhomogeneity has stiffness  $E = E_0 + \Delta E$ . The vibration patterns of the medium, with and without the inhomogeneity, are derived from the vector displacement equations.

The wave motion equation can be expressed in term of the displacements as:

$$\frac{E}{2(1+\nu)(1-2\nu)} \nabla \nabla \cdot \bar{\mathbf{u}} + \frac{E}{2(1+\nu)} \nabla^2 \bar{\mathbf{u}} = \rho \frac{\partial^2 \bar{\mathbf{u}}}{\partial t^2}, \quad (1)$$

where  $E$ ,  $\nu$ ,  $\rho$  and  $\bar{\mathbf{u}}$  are the Young's modulus, Poisson's ratio, mass density and displacement vector, respectively. The above motion equation can be decomposed into two decoupled motion equations, one governing longitudinal wave motion, and the other governing shear wave motion. Only the shear wave equation is chosen for consideration, for the following reasons. First, the longitudinal waves have wavelengths much larger than organs of interest at the frequencies used in sonoelastography (Parker et al. 1992). In addition, biological tissue is nearly incompressible, so the Poisson's ratio approaches 0.5 (Fung 1981; Parker et al. 1990). At this Poisson's ratio, the wave dilatation that represents the longitudinal wave motion is close to zero; thus, the shear wave motion  $\bar{\mathbf{u}}_T$  dominates the wave propagation. In a homogeneous medium, the shear wave component is governed by the wave equation (Gao et al. 1995):

$$\frac{E}{2(1+\nu)} \nabla^2 \bar{\mathbf{u}}_T = \rho \frac{\partial^2 \bar{\mathbf{u}}_T}{\partial t^2}. \quad (2)$$

The shear wave eqn (2) for the medium with inhomogeneity is expressed as:

$$\nabla^2 \bar{\mathbf{u}}_T - \frac{1}{C_0^2(1+\gamma)} \frac{\partial^2 \bar{\mathbf{u}}_T}{\partial t^2} = 0, \quad (3)$$

where

$$C_0 = \left[ \frac{E_0}{2\rho(1+\nu)} \right]^{1/2}, \quad (4)$$

and

$$\gamma = \frac{E - E_0}{E_0}. \quad (5)$$

$E_0$  is Young's modulus of the homogeneous background material where  $\gamma = 0$ .  $E$  is Young's modulus of the inhomogeneous material where  $\gamma \neq 0$ .  $\gamma > 0$  indicates a hard lesion and  $\gamma < 0$  indicates a soft lesion. Biological tissue is lossy and typically modeled as a viscoelastic material (Fung 1981). Therefore, a relaxation term should be included in eqn (3) (Kinsler et al. 1982). Assuming that the external vibration has a harmonic time dependence  $\bar{\mathbf{u}}_T = \bar{\mathbf{U}} \exp(i\omega t)$ , eqn (3) with a loss term becomes:

$$\nabla^2 \bar{\mathbf{U}} + \frac{K^2}{(1+\gamma)} \bar{\mathbf{U}} - \frac{iK^2}{Q_0(1+\gamma)} \bar{\mathbf{U}} = 0, \quad (6)$$

where  $K = \omega/C_0$  and  $Q_0$  is the  $Q$  factor of the system at the frequency  $\omega$ .

There is no closed form solution to eqn (6). To gain insight into the effect of the inhomogeneity on the wave fields, the "elastic-Born" approximation is used to rearrange the governing equations (Gao et al. 1995). The motion field is decomposed into an incident wave and a scattered wave:

$$\bar{\mathbf{U}} = \bar{\mathbf{U}}_i + \bar{\mathbf{U}}_s. \quad (7)$$

The incident wave satisfies the homogeneous wave equation:

$$\nabla^2 \bar{\mathbf{U}}_i + K^2 \bar{\mathbf{U}}_i - \frac{iK^2}{Q_0} \bar{\mathbf{U}}_i = 0, \quad (8)$$

and the given boundary conditions. The scattered wave due to the inhomogeneity satisfies:

$$\nabla^2 \bar{\mathbf{U}}_s + K^2 \bar{\mathbf{U}}_s - \frac{iK^2}{Q_0} \bar{\mathbf{U}}_s = \beta K^2 \left( 1 - \frac{i}{Q_0} \right) \bar{\mathbf{U}}_i, \quad (9)$$

where the function  $\beta$  is defined as:

$$\beta = \frac{\gamma}{1+\gamma} = \frac{E - E_0}{E}. \quad (10)$$

This source term  $\beta$  governs the strength of the perturbation from an otherwise homogeneous solution. Thus, for a point inhomogeneity in an infinite medium, the scattered wave increases proportionally to the term  $\beta(x, y)$ . The relation between the two parameters  $\beta$  and  $E/E_0$  is

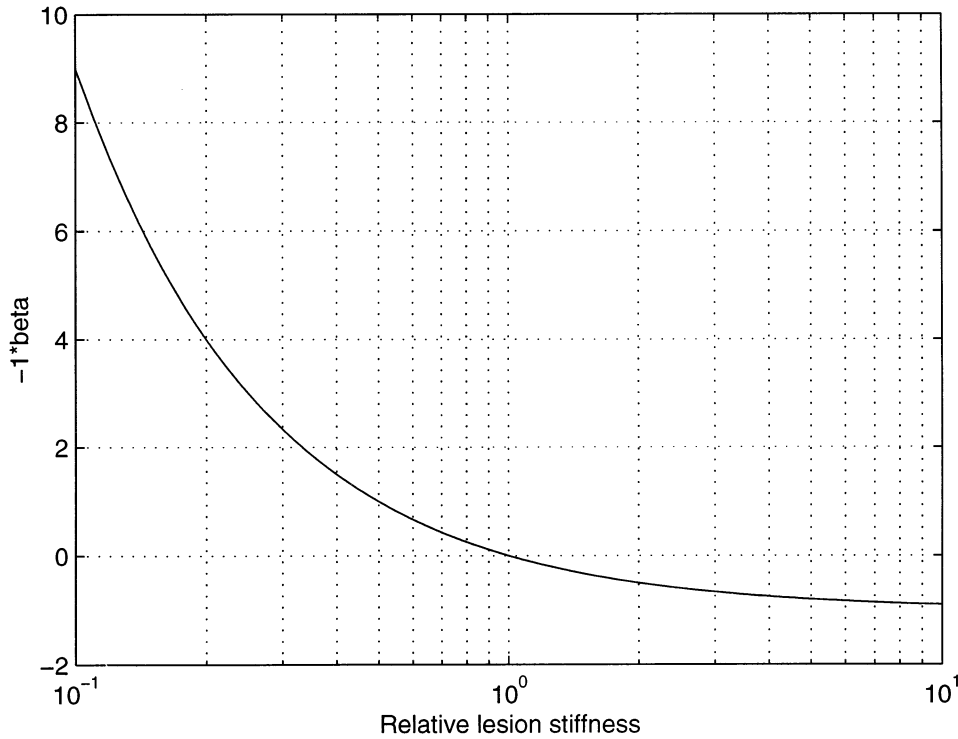


Fig. 1. The relation between the two parameters  $\beta$  and  $E/E_0$  ( $\beta$  is the strength of the source term in the derivation of the “elastic-Born” equation).

shown in Fig. 1. Note the leveling off of  $\beta$  as  $E/E_0 \rightarrow \infty$ ; that is, as the inhomogeneity becomes extremely stiff. However, the assumptions involved in deriving the “elastic-Born” equation limit the range of applicability of the equations to some limited range of  $E/E_0$  near unity. Gao *et al.* (1995) obtained solutions for simplified geometry, and showed that a small hard lesion produced a localized reduction of displacement in a vibration pattern. This concept will be quantified in the following sections.

**FINITE ELEMENT ANALYSES**

The finite element method (FEM) is a numerical procedure for analyzing structures and continua. In our work, the FEM is adopted as a tool to obtain a discrete approximation to the 2-D and 3-D viscoelastic vibration problems with arbitrary boundaries. Equations that govern the dynamic response of a medium are derived by requiring the work of external vibration forces to be absorbed by the work of internal, inertial and viscous forces for any small admissible motion. For a single element, the equilibrium equation for the harmonic motion case is expressed as (Cook *et al.* 1989):

$$-\omega^2[m]\{d\} + i\omega[c]\{d\} + [k]\{d\} = \{r^{ext}\}, \quad (11)$$

where  $[m]$ ,  $[c]$  and  $[k]$  are the element mass, damping and stiffness matrices, respectively, and  $\{d\}$  and  $\{r^{ext}\}$

are the element grid displacement amplitude vector and the element external force amplitude vector, respectively, and  $\omega$  is the angular vibration frequency. The damping matrix is proportional to the structural damping coefficient  $b$ . The damping ratio  $\xi$  is related to damping coefficient  $b$  at the vibration frequency  $\omega$  by the expression:

$$\xi = \frac{\omega b}{2E}. \quad (12)$$

After assembly of elements, the governing equation in the FEM is derived from eqn (11):

$$-\omega^2[M]\{D\} + i\omega[C]\{D\} + [K]\{D\} = \{R^{ext}\}, \quad (13)$$

where  $[M]$ ,  $[C]$  and  $[K]$  are the assembled mass, damping and stiffness matrices, respectively, and  $\{D\}$  and  $\{R^{ext}\}$  are the assembled grid displacement amplitude vector and the assembled external force amplitude vector, respectively. Solution of eqn (13) results in the grid displacements of the structure due to a known external harmonic excitation.

In this section, we describe use MSC/NASTRAN (MacNeal-Schwendler Corporation, Los Angeles, CA), a commercial FEM package, to systematically investi-

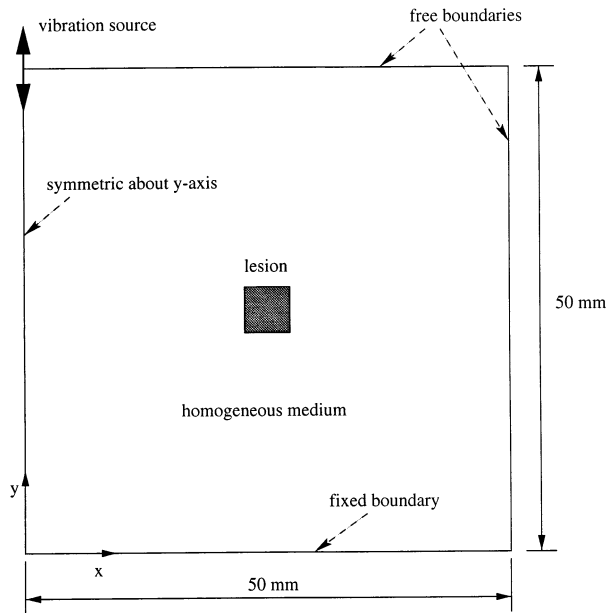


Fig. 2. Diagram of 2-D model for the FEM simulation.

gate the lesion detectability. Effects of parameters, including lesion stiffness, vibration frequency, lesion size and material damping on the resulting wave motion were investigated. A 2-D model was first considered to obtain systematic results for the parameter studies. Later, a 3-D phantom was modeled to observe lesion visibility and to compare with the experimental results for a tissue-mimicking phantom.

#### 2-D FEM model

A 2-D domain is shown in Fig. 2. For simplicity, it is assumed that the domain is symmetric about the  $y$  axis and the shape of the lesion is square. A time-harmonic point vibration source with displacements in the  $y$  direction is applied on the top surface in the plane of symmetry. The bottom boundary is fixed in all directions and the other boundaries are free. The 2-D domain shown in Fig. 2 is uniformly meshed using 2500 bilinear isoparametric elements with a 1-mm grid spacing. The resulting vertical ( $y$  direction) displacement fields are compared with and without the lesion.

The following parameters are defined for explanation of the results:

$d$ —The average vertical displacement amplitude within the lesion region.

$d_0$ —The average vertical displacement amplitude within the region corresponding to the lesion, but in a homogeneous model.

The average displacement amplitude is calculated by averaging the displacement amplitudes of all the grids within the region considered.

The ratio  $E/E_0$  represents the relative stiffness of the lesion with respect to the homogeneous medium. The ratio  $d/d_0$  represents the relative displacement amplitude of the lesion with respect to the otherwise homogeneous medium. The value of  $d/d_0$  will be used in this paper as a measure of the lesion detectability in sonoelastography, and is the key parameter of interest throughout this paper. Results show generally that  $d/d_0 < 1$  for hard lesions,  $d/d_0 = 1$  in absence of a lesion and  $d/d_0 > 1$  for soft lesions. In the following, we investigate the dependence of lesion detectability on lesion stiffness, vibration frequency, lesion size and material damping coefficients. Both the amplitude and phase are considered in the following analyses. The grey-scale images of the absolute vertical displacement amplitudes were used to provide visual representation of the predicted motions. Each image uses 8 bits dynamic range.

Figure 3 shows the relationship between  $d/d_0$  and  $E/E_0$  for different vibration frequencies, where the lesion size is  $6 \text{ mm} \times 6 \text{ mm}$ ,  $E_0 = 20 \text{ kPa}$ , and the damping ratio  $\xi = 0.02$ . The general trend of each curve is similar to that for  $\beta$  given in Fig. 1, except in the region  $E/E_0 \ll 1$ ; in this region, the “elastic-Born” approximation would no longer be valid. The results indicate that the detectability increases with the increase of relative lesion stiffness when  $E/E_0 > 1$  and with the decrease of relative lesion stiffness when  $E/E_0 < 1$ . When the elasticity of the inhomogeneity is 3 times that of the surrounding homogeneous medium, the decrease of the tumor displacement is over 20% for a frequency greater than 400 Hz. Figure 4 displays and compares the vibration patterns at 400 Hz for a soft lesion with  $E/E_0 = 0.2$ , a homogeneous medium and a hard lesion with  $E/E_0 = 5$ . Compared with the homogeneous medium in Fig. 4 (center), the soft lesion region is brighter in the grey-scale amplitude image (left) and the hard lesion region is darker (right). The lesion causes the localized disturbance of the vibration pattern and identifies itself in the image. Note that the six distinct bright dots in Fig. 4 (left) show the vibration pattern with a shorter wave length in the soft lesion region, as expected.

Figure 3 also shows the trend of lesion detectability when the vibration frequencies change. Theory, eqn (9), predicts that the strength of the inhomogeneous source term increases as  $\beta K^2$ , thus increasing with frequency. Figure 3 demonstrates that the change in  $d/d_0$  increases as frequency increases. The grey-scale images for visualization of the vibration patterns are presented in Fig. 5a, b, c, d. For 300-Hz, 400-Hz and 600-Hz vibration, the tumor is clearly visible in the images, and the detectability increases with the vibration frequency in this frequency range. For the frequency 100 Hz, the lesion cannot be easily identified.

There are no discontinuities in the displacement

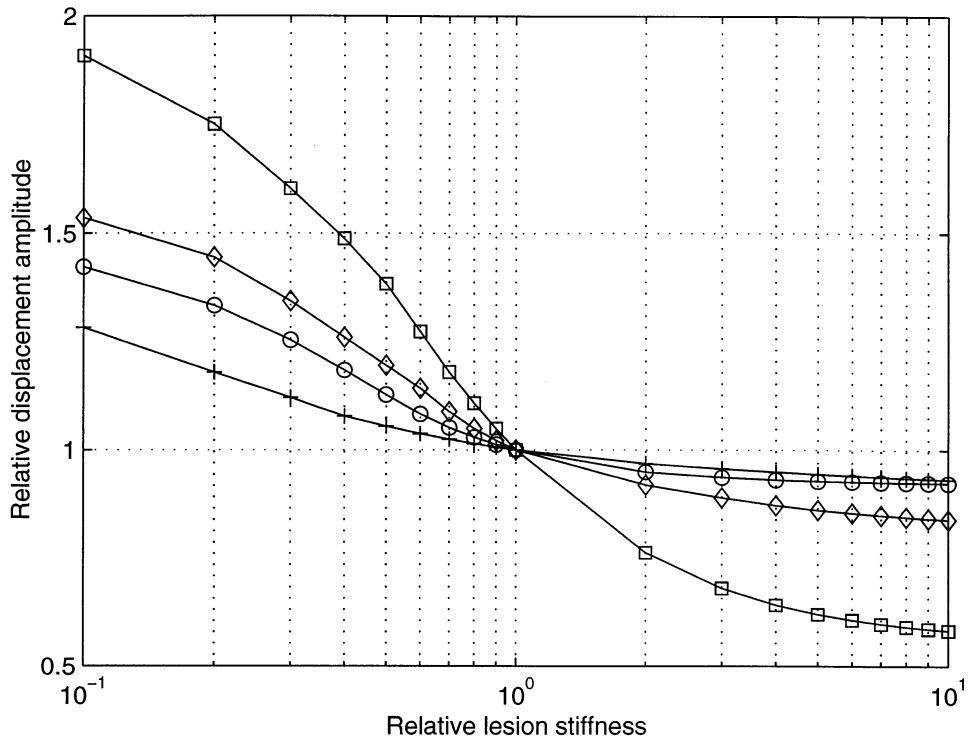


Fig. 3. Relative displacement amplitude  $d/d_0$  vs. relative lesion stiffness  $E/E_0$  from the FEM study (+ = 60 Hz; circle = 100 Hz; diamond = 300 Hz; square = 400 Hz). The lesion size is 6 mm × 6 mm. Note that the general trend follows the theoretical derivation of the  $\beta$  term as shown in Fig. 1.

field, even at the lesion boundaries, although the lesion and the background material have different elasticities. Therefore, the vibration amplitude imaging technique is not suitable for small lesion detection at very low frequencies (below 200 Hz). Instead, strain imaging may be useful in this case. Given the external forces, the strain is proportional to the material elasticity because the stress is continuous at the boundary between the lesion and the homogeneous medium. Thus, the strain in the lesion region differs from that in the background media. Figure

6 compares the strain images for a homogeneous and inhomogeneous ( $E/E_0 = 5$ ) medium at 100 Hz, where the brightness is proportional to the vertical strain component. At this low frequency, the lesion in the strain image is much more evident than that in the displacement amplitude image in Fig. 5a. However, because strain estimations require derivative operators, the strain image will be sensitive to noise. Although the strain image is promising, this paper concentrates on the displacement image technique.

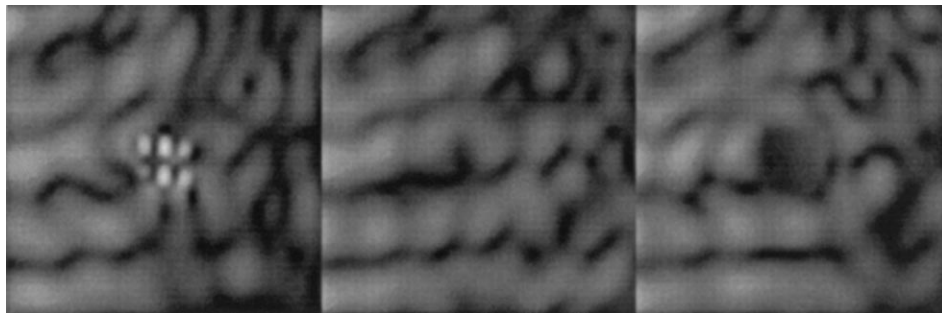


Fig. 4. Grey-scale images of the vertical displacement amplitudes at 400 Hz vibration. Each image is 40 mm width by 40 mm height, and is a region of interest within the domain shown in Fig. 2. The lesion size is 6 mm × 6 mm. (left) Soft lesion  $E/E_0 = 0.2$ ; middle = no lesion; right = hard lesion  $E/E_0 = 5$ .

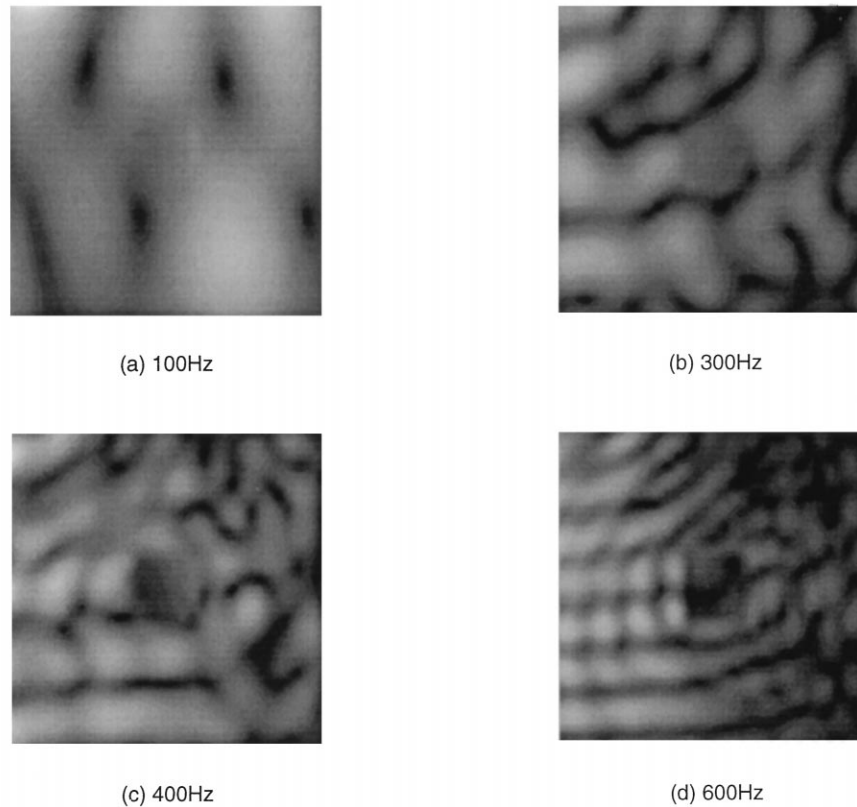


Fig. 5. Grey-scale images of the vertical displacement amplitudes for  $E/E_0 = 5$  at various vibration frequencies. Each image size is the same as those in Fig. 4. The lesion size is  $6 \text{ mm} \times 6 \text{ mm}$ .

So far, only the amplitude of the vibration motion field has been considered. The phase may also be useful in determining the viscoelastic properties of a material (Yamakoshi et al. 1990; Levinson et al. 1995). The phase color maps at 600 Hz for the homogeneous and for the

hard lesion  $E/E_0 = 5$  are sketched in Fig. 7. It is a visual representation of spatial changes of phase of the vibration motion field. The color model of intensity, hue and saturation (HIS) is converted to RGB color model. Here, both the intensity and saturation are set to 1, and the hue

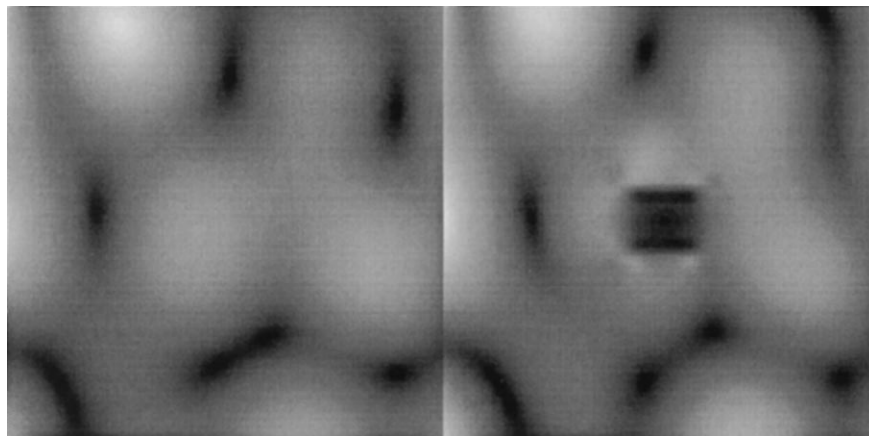


Fig. 6. The strain images at 100 Hz vibration frequency: (left) homogeneous; (right) inhomogeneous. The inhomogeneous case was derived from the displacement amplitude image of Fig. 5a with  $E/E_0 = 5$ .

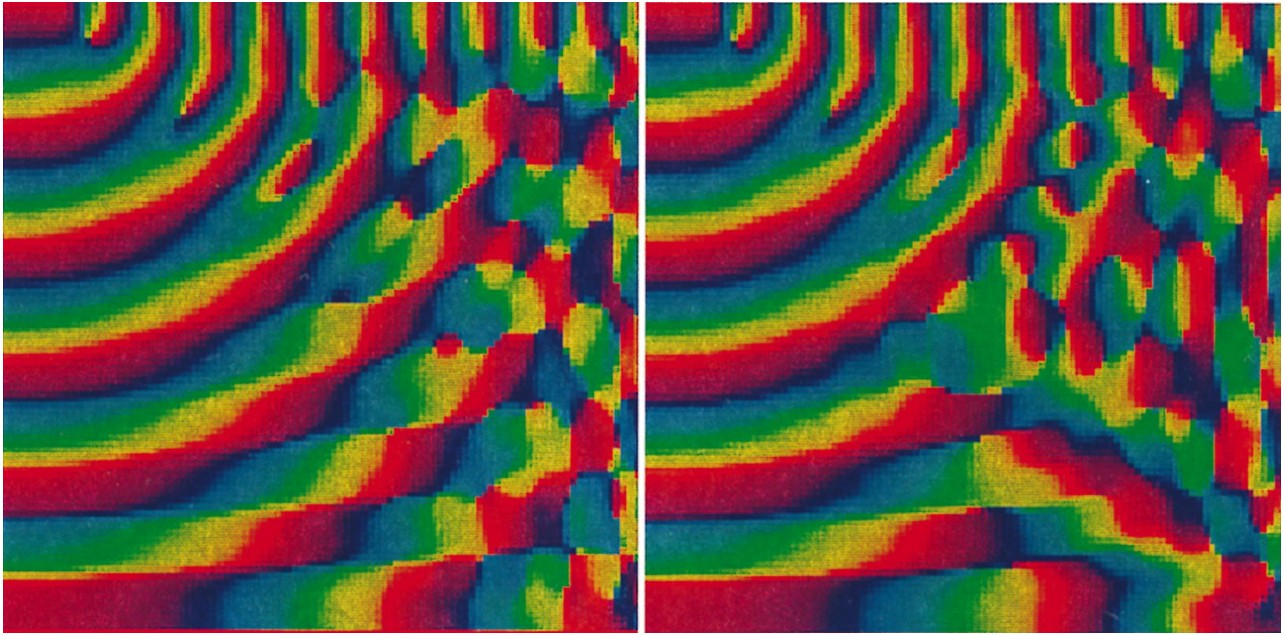


Fig. 7. Phase color map at 600 Hz for the homogeneous case on the left and for the 6 mm  $\times$  6 mm hard lesion with  $E/E_0 = 5$  on the right.

represents the phase, which has a range from 0 to 360°. The lesion can be identified in the center of the static image of Fig. 7, but is much more clearly visualized in the animation of a phase color-map sequence.

The detectability of a lesion also depends on its size or volume. Figure 8 shows how the detectability depends on lesion size for an excitation frequency of 400 Hz. The detectability increases dramatically when the lesion size increases. The grey-scale vibration images for different lesion sizes are displayed in Fig. 9 for the case  $E/E_0 = 5$ . The lesion size is (left) 4 mm  $\times$  4 mm; (middle) 6 mm  $\times$  6 mm; and (right) 8 mm  $\times$  8 mm. A large lesion causes a large disturbance region, so the lesion visibility is better. A small lesion with size 4 mm  $\times$  4 mm is thought to be detectable because the darker lesion region in the image can be identified.

The exact amount of loss and its frequency-dependence in tissue at these frequencies is unknown. However, we can predict the effect of damping by numerical simulation. Figure 10 shows that the lesion detectability decreases with increasing damping ratio. For a purely elastic case, the average lesion displacement is 80% below the corresponding average displacement in a homogeneous medium. Even for a small damping ratio equal to 0.02, there is a decrease in lesion detectability. *In vivo* measurements will be required to determine the damping ratios of tissues and how they increase with vibration frequency.

From the above observations and analyses of the 2-D FEM simulation results, the recommended frequen-

cies for lesion detection range from approximately 200 Hz to 600 Hz, assuming a lesion with  $E/E_0 > 3$  and a characteristic dimension (*e.g.*, diameter) of at least 4 mm.

### 3-D FEM model

The above analyses for the 2-D model present some quantitative results pertaining to lesion detectability. These systematic results verify the theory discussed in the preceding section and provide insight into sonoelastography. In this section, a more complex 3-D FEM model is used to simulate a tissue-mimicking phantom experiment.

The phantom model for 3-D FEM simulation is shown in Fig. 11. The actual phantom has four spherical lesions at different locations. To establish a computable simulation model, some simplifications and assumptions are made. First, only one lesion is considered for the mesh simplicity of the model, as indicated in Fig. 11. Because the sizes of the lesions are very small compared with the phantom, and the four lesions are well separated, the results due to the simplification will not cause a large error. Second, the vibration surface source is applied along the plane of symmetry; thus, only half the phantom including half the lesion needs to be modeled. The lesion shape is assumed to be a cube for easier meshing with the FEM. The volume of the simulated lesion is set equal to the volume of the actual spherical lesion. The measured Young's modulus and damping coefficient are used in the FEM model. The stiffness of

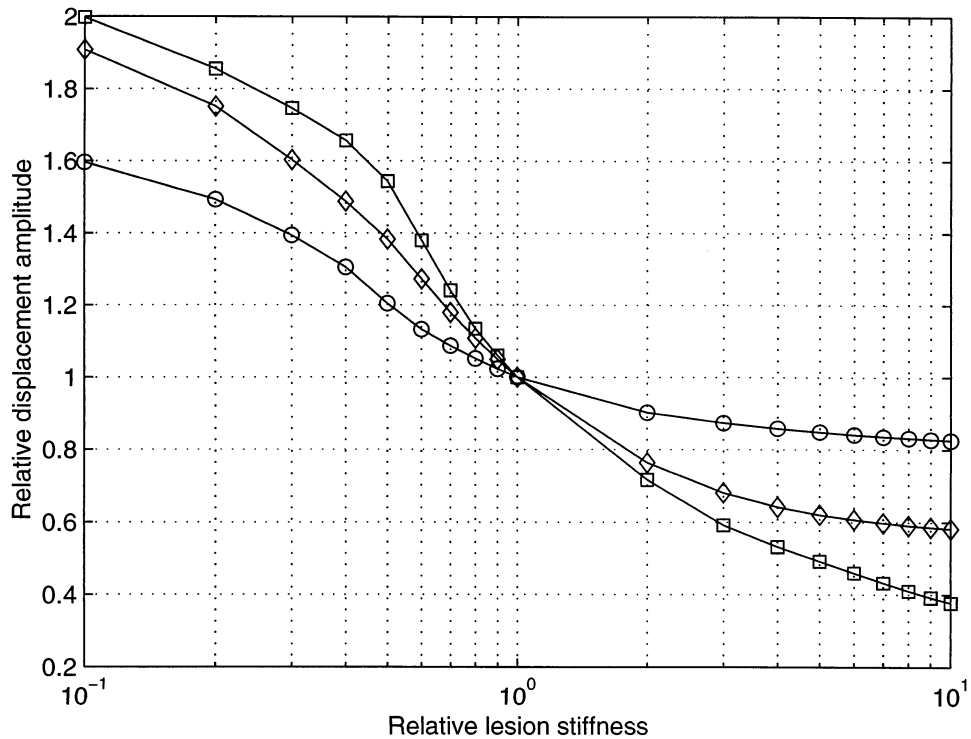


Fig. 8. Relative displacement amplitude  $d/d_0$  vs. relative lesion stiffness  $E/E_0$  at vibration frequency 400 Hz for different size lesions: circle = 4 mm  $\times$  4 mm; diamond = 6 mm  $\times$  6 mm; square = 8 mm  $\times$  8 mm.

the lesion is 7 times that of the homogeneous material of the phantom. The model is adaptively meshed with approximately 15,000 3-D hexahedral isoparametric elements, where the mesh is finer in the region close to the lesion and coarser elsewhere. The lesion is meshed by 16 elements. The FEM mesh model provides adequate resolution over the vibration frequency range of interest.

The grey-scale images obtained from the simulation data in the region of interest are shown in Fig. 12a and b for 248 Hz and 318 Hz, respectively. The cubic spline interpolation is performed on the FEM data before dis-

playing the image, so that the images have higher spatial sampling. The shape of the phantom and the boundary conditions are complicated, so the vibration pattern is not simple. However, the lesion regions are readily located. The images will be compared with the experimental results.

## EXPERIMENTAL RESULTS

The tissue-mimicking phantom in our experiments was manufactured by Computerized Imaging Reference



Fig. 9. Grey-scale images of the vertical displacement amplitudes at a vibration frequency 400 Hz for different size lesions where  $E/E_0 = 5$ : left = 4 mm  $\times$  4 mm; middle = 6 mm  $\times$  6 mm; right = 8 mm  $\times$  8 mm.

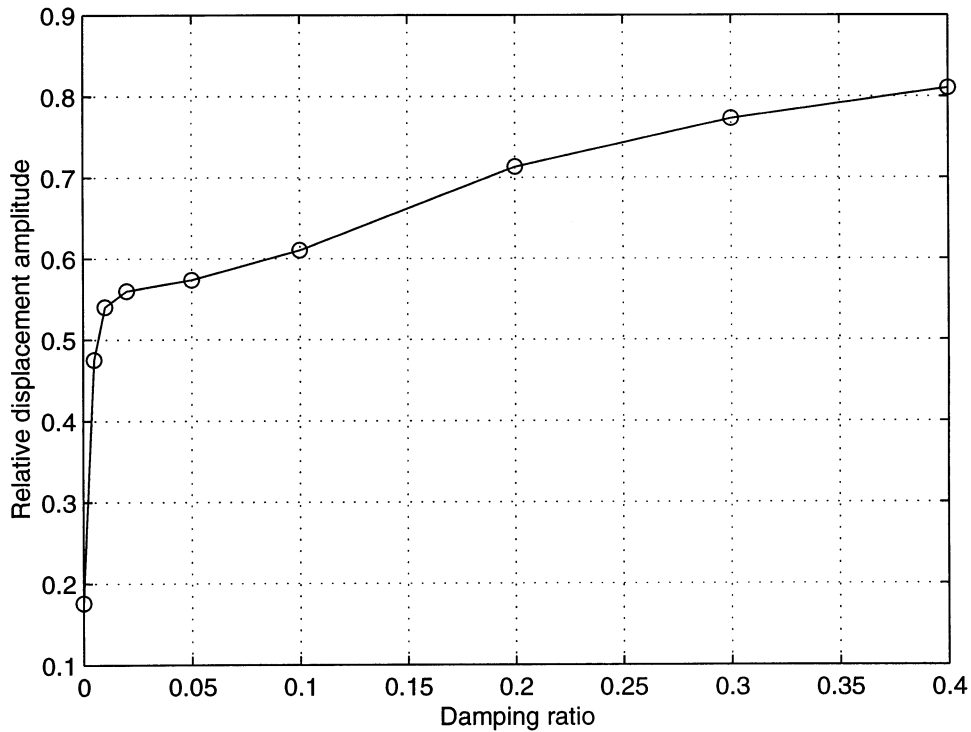


Fig. 10. The relation between the lesion detectability and material damping ratio for  $E/E_0 = 5$  at 400 Hz.

System Inc. (CIRS, Norfolk, VA). The specifications for the phantom were that the phantom materials reproduce the ultrasonic appearance of liver tissue and the simulated tumors are isoechoic on B-scan images. It was also specified that the lesions be 7 times stiffer than the background materials. CIRS successfully made a phantom consisting mainly of Zerdine that contains 4 lesions. The half phantom shape is sketched in Fig. 11.

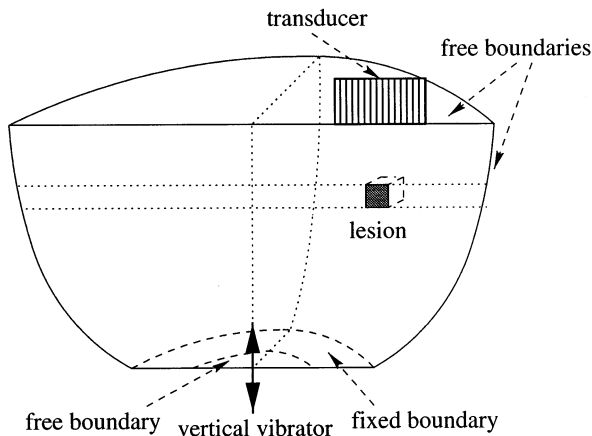


Fig. 11. Diagram of the phantom model for the 3-D FEM simulation.

*Measurement of elasticity and viscosity*

The numerical simulations assumed viscoelastic material properties to approximate the mechanical properties of biological tissue. We measured the values of the elasticity and viscosity of the tissue-mimicking phantom. In practice, Poisson's ratio is difficult to measure accurately. A value of 0.495 is assumed because tissue is nearly incompressible (Fung 1981; Parker *et al.* 1990). Small hard and soft circular cylindrical samples were ordered together with the phantom. The hard and soft samples have the same mechanical and acoustical properties as the hard lesion and background material in the phantom, respectively. Two experiments were used to measure the Young's modulus for each sample. A simple load cell was first used to statically compress a small circular cylindrical sample. Both the top and bottom surfaces of the sample were lubricated with vegetable oil to approximate a free slip boundary to create a uniform stress state within the sample. Young's modulus in a certain strain range can be calculated from the slopes of plots of stress vs. strain. Measured values of Young's modulus for different strain levels are given in Table 1 for both the homogeneous background material and the lesion material. The ratio of elasticities of the two materials is approximately equal to 7 at various strains, which corresponds to the manufacturing specification.

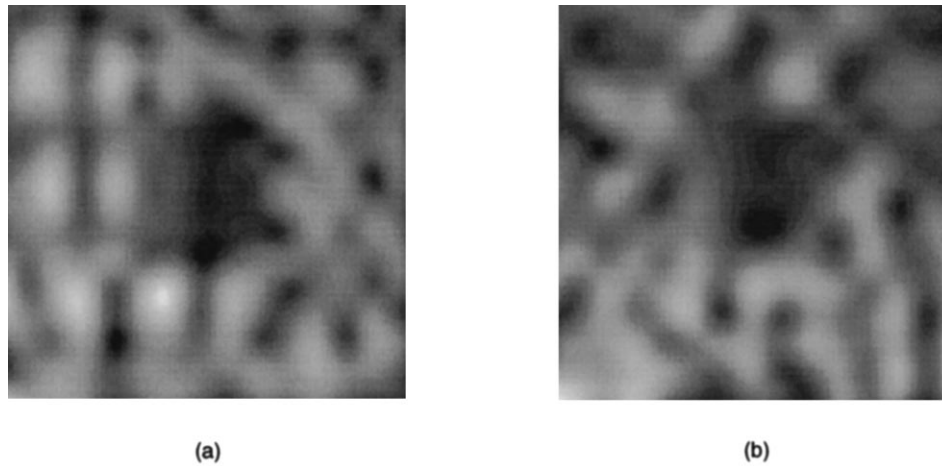


Fig. 12. Grey-scale images of the vertical displacement amplitudes for from the 3-D FEM simulation: (a) 248 Hz; (b) 318 Hz. The 1-cm lesion  $E/E_0 = 7$  is located at the center of the region of interest shown.

The small strain range was chosen so that the basic linear elastic equations were satisfied. The viscosity cannot be obtained from the static measurement. Both elasticity and viscosity were measured using a sensitive dynamic measurement instrument (Solids Analyzer RSA-II). Because of equipment limitations, data could be obtained only from 1 Hz to 15 Hz. The Young's modules and the damping ratio measured for the background material were about 21 kPa and 0.02 at the strain 0.05 within this vibration frequency range.

#### *Sonoelastography experiments*

The spherical lesions imbedded in the phantom result in the boundary between the lesion and the background material. Because the lesion is isoechoic, the boundary is barely detectable. However, the high-resolution GE Logiq 700 scanner used in the experiments can sometimes display a very faint trace of the boundary in B-scan mode. This is used to confirm the lesion position for the experiment setup.

The experiment setup is consistent with the simulation model in Fig. 11. Vibration Test System Corporation (VTS, Cleveland, Ohio) supplied a point vibration source system. A 9-MHz linear transducer probe (a 739L GE Medical) was used to locate the lesion of interest in

the phantom. The lesion corresponding to the 3-D FEM model was selected for detection. Once this lesion was located, the transducer position was adjusted such that its orientation was in the symmetry plane. The point vibrator was applied at the center of the bottom surface. The color Doppler mode of the GE Logiq 700 ultrasound system was used to perform the experiment. A Doppler spectral variance estimator was utilized to determine vibration amplitudes (Huang et al. 1990, 1992). After the color-flow parameters were set appropriately, the vibrator was turned on and adjusted to increase the vibration amplitude until the color Doppler signal covered the background. Then a void or vacancy occurred over the region of the lesion. In this way, a sonoelastogram of the isoechoic lesion was produced.

The phantom experiments were performed at vibration frequencies 248 Hz and 318 Hz, respectively. The color Doppler data were obtained by data transfer from the GE Extend program. The results are shown in Fig. 13a, b. The void in the images indicates the existence of the hard lesion. The phantom experimental results in Fig. 13 agree well with the vibration pattern of the FEM simulation in Fig. 12.

## CONCLUSIONS

In this paper, lesion detectability in vibration sonoelastography was investigated, using theoretical equations, finite element analyses and experimental tests on a tissue-mimicking phantom. The theoretical equations established the basic concepts and mechanisms for sonoelastography. The 2-D FEM model was used to study the lesion detectability as a function of lesion size, vibration frequency, material elastic properties and damping, and the results were consistent with the predictions of the

Table 1. The measured Young's modulus for various strain levels

Strains	0.02	0.03	0.04	0.05
Background $E_0$ (kPa)	13	17	18	19
Lesion $E$ (kPa)	94	120	130	132
Ratio $E/E_0$	7.2	7.1	7.2	6.9

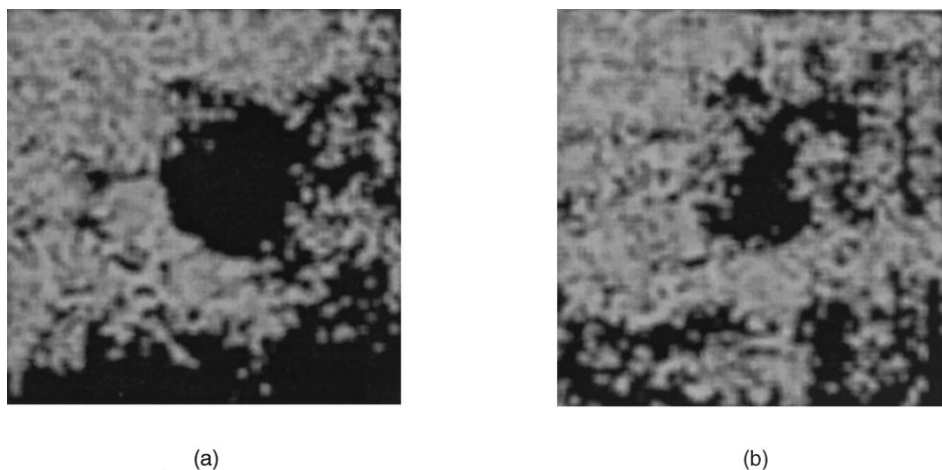


Fig. 13. Real-time sonoelastography images of the vertical displacement amplitudes from the phantom experiments: (a) 248 Hz; (b) 318 Hz. The 1-cm diameter stiff lesion  $E/E_0 = 7$  was located slightly to the right of center of the region of interest shown.

theory. The systematic and quantitative 2-D results showed that detectability increases with lesion stiffness and size. For the cases considered, detectability increased with the vibration frequency in a certain range. However, the damping mechanism ultimately limits the penetration of high-vibration frequencies. Small lesions are not easily detected at very low frequencies (below 200 Hz) using the vibration-amplitude imaging technique. Instead, the strain imaging technique may be used for lesion detection at very low-frequency vibration. A tissue-mimicking phantom was numerically simulated with the 3-D FEM model. The experiments were performed on the phantom using advanced Doppler imaging techniques. The experimental results corresponded well with the predictions of the 3-D FEM simulations. The results presented in this paper provide guidelines for clinical application of vibration sonoelastography or for any coherent imaging system capable of measuring vibration within tissue.

*Acknowledgements*—This work was supported in part by the NSF/NYS center for electronic imaging system, and by NIH. The loan of equipment from GE Medical Systems is gratefully acknowledged. The authors especially thank Drs. Kai Thomenius and Anne Hall of GE for their insightful advice. We are grateful to Heather Miller of CIRS for her assistance with the phantom design and testing.

## REFERENCES

- Cook RD, Malkus DS, Plesha ME. Concepts and application of finite element analysis. New York: John Wiley & Sons Inc., 1989:368–370.
- Fung YC. Biomechanics—Mechanical properties of living tissues. New York: Springer-Verlag, 1981.
- Gao L, Parker KJ, Alam SK, Lerner RM. Sonoelasticity imaging: Theory and experimental verification. *J Acoust Soc Am* 1995;97:3875–3886.
- Gao L, Parker KJ, Alam SK, Rubens D, Lerner RM. Theory and application of sonoelasticity imaging. *Int J Imaging Syst Technol* 1997;8:104–109.
- Gao L, Parker KJ, Lerner RM, Levinson SF. Elastic imaging of tissue—a review. *Ultrasound Med Biol* 1996;22:959–977.
- Huang SR, Lerner RM, Parker KJ. On estimating the amplitude of harmonic vibration from the Doppler spectrum of reflected signals. *J Acoust Soc Am* 1990;88:310–317.
- Huang SR, Lerner RM, Parker KJ. Time domain Doppler estimators of the amplitude of vibrating targets. *J Acoust Soc Am* 1992;91:965–974.
- Kinsler LE, Frey AR, Coppens AB, Sanders JV. Fundamentals of acoustics. New York: John Wiley & Sons Inc., 1982:90–91.
- Lerner RM, Huang SR, Parker KJ. Sonoelasticity images derived from ultrasound signals in mechanically vibrated tissues. *Ultrasound Med Biol* 1990;16:231–239.
- Lerner RM, Parker KJ, Holen J, Gramiak R, Waag RC. Sonoelasticity: Medical elasticity images derived from ultrasound signals in mechanically vibrated targets. *Acoust Imaging* 1988;16:317–327.
- Levinson SF, Shinagawa M, Sato T. Sonoelastic determination of human skeletal muscle elasticity. *J Biomechan* 1995;28(10):1145–1154.
- O'Donnell M, Skovoroda AR, Shapo BM, Emelianov SY. Internal displacement and strain imaging using ultrasonic speckle tracking. *IEEE Trans Ultrason Ferroelec Freq Contr* 1994;41:314–325.
- Ophir J, Cespedes I, Ponnekanti H, Yazdi Y, Li X. Elastography: a quantitative method for imaging the elasticity of biological tissues. *Ultrason Imaging* 1991;13:111–134.
- Ophir J, Kallel F, Varghese T, Bertrand M, Cespedes I, Ponnekanti H. Elastography: A systems approach. *Int J Imaging Syst Technol* 1997;8:89–103.
- Parker KJ, Lerner RM. Sonoelasticity of organs: shear waves ring a bell. *J Ultrasound Med* 1992;11:387–392.
- Parker KJ, Huang SR, Musulin RA, Lerner RM. Tissue response to mechanical vibrations for sonoelasticity imaging. *Ultrasound Med Biol* 1990;16:241–246.
- Skovoroda AR, Emelianov SY, Lubinski MA, Sarvazyan AP, O'Donnell M. Theoretical analysis and verification of ultrasound displacement and strain imaging. *IEEE Trans Ultrason Ferroelec Freq Contr* 1994;41:302–313.
- Yamakoshi Y, Sato J, Sato T. Ultrasonic imaging of internal vibration of soft tissue under forced vibration. *IEEE Trans Ultrason Ferroelec Freq Contr* 1990;37:45–53.